ATMOSPHERIC SCIENCE

Unexpected significance of a minor reaction pathway in daytime formation of biogenic highly oxygenated organic compounds

Hongru Shen[1], Luc Vereecken[2], Sungah Kang[2], Iida Pullinen[2]†, Hendrik Fuchs[2,3], Defeng Zhao[1,4,5,6]*, Thomas F. Mentel[2]

Secondary organic aerosol (SOA), formed by oxidation of volatile organic compounds, substantially influence air quality and climate. Highly oxygenated organic molecules (HOMs), particularly those formed from biogenic monoterpenes, contribute a large fraction of SOA. During daytime, hydroxyl radicals initiate monoterpene oxidation, mainly by hydroxyl addition to monoterpene double bonds. Naturally, related HOM formation mechanisms should be induced by that reaction route, too. However, for α-pinene, the most abundant atmospheric monoterpene, we find a previously unidentified competitive pathway under atmospherically relevant conditions: HOM formation is predominately induced via hydrogen abstraction by hydroxyl radicals, a generally minor reaction pathway. We show by observations and theoretical calculations that hydrogen abstraction followed by formation and rearrangement of alkoxy radicals is a prerequisite for fast daytime HOM formation. Our analysis provides an accurate mechanism and yield, demonstrating that minor reaction pathways can become major, here for SOA formation and growth and related impacts on air quality and climate.

INTRODUCTION

Secondary organic aerosols (SOAs) in the atmosphere affect air quality and climate by contributing a large portion to the mass of submicrometer particulate matter (*1*–*3*), by acting as cloud condensation nuclei, and by scattering and absorbing solar radiation (*4*–*9*). SOA is formed by condensation of products from the atmospheric oxidation of volatile organic compounds (VOCs) (*3*, *10*). Here, highly oxygenated organic molecules (HOMs) play a pivotal role (*11*–*17*) because of their low volatility. New particles can be formed from HOMs and be grown to sizes where they can act as cloud condensation nuclei. Elucidating HOM formation pathways is thus crucial to assess and predict the abundance of SOA and its impact on climate and air quality.

HOMs typically contain at least six oxygen atoms (*18*) and were first found in the reaction of alkenes with ozone (*11*–*13*), a common atmospheric oxidant, after several autoxidation steps (*18*, *19*) involving intramolecular H-shifts with subsequent O_2 addition as shown in fig. S1. Bimolecular termination reactions of the HOM peroxy radicals lead to several product families $C_ZH_YO_X$, wherein we define a family as molecules having the same C_ZH_Y backbone but a varying number X of O-atoms. In particular, biogenic monoterpenes are found to efficiently form HOM (*11*, *20*–*22*) and to contribute substantially to SOA formation (*11*–*13*, *20*, *23*) owing to their high emission rates (*24*). As shown for the most abundant monoterpene α-pinene ($C_{10}H_{16}$), also hydroxyl radicals (OH), the most important atmospheric oxidants, initiate fast HOM formation via a family of peroxy radicals (RO_2•) containing 10 C-atoms and 17 H-atoms ($C_{10}H_{17}O_X$•) (*25*–*27*). Here, we report a previously unidentified pathway for OH-induced HOM formation via $C_{10}H_{15}O_X$•, intermediates with only 15 H-atoms as an alternative to previously proposed chemical pathways (*25*–*27*). Notably, on the basis of currently known formation pathways of HOM, such intermediates with 15 H-atoms are expected to be produced from only the reaction of α-pinene with ozone (*11*–*13*, *20*, *23*) or oxidation of α-pinene oxidation products by OH (*28*, *29*).

Only few studies have investigated HOM formation induced solely by OH radicals, although oxidation by OH radicals formed from the ozonolysis reaction itself inherently contributes to HOM formation. While HOM yields have been determined in the α-pinene oxidation by OH (*11*, *12*, *21*, *26*) and several HOM products have been reported, product distributions and formation mechanisms remain unclear. OH-initiated HOM formation was believed to start with OH addition to the C=C double bond of α-pinene forming peroxy radicals with 10 C-atoms and 17 H-atoms ($C_{10}H_{17}O_3$•) (*25*–*27*). Berndt *et al.* (*26*) identified a number of HOM products formed via $C_{10}H_{17}O_X$• peroxy radicals, related to each other by autoxidation steps. They proposed a mechanism where OH addition is followed by opening of the four-membered ring and forming a hydroxy peroxy radical containing a new C=C double bond in the six-membered ring (*29*, *30*). Recently, Xu *et al.* (*27*) calculated fast rates (>0.1 s^{-1}) for unimolecular H-shifts in such RO_2• radicals and proposed this pathway to be a major channel of HOM formation in the OH oxidation of α-pinene. However, only less oxygenated products ($O \leq 5$) were characterized by Xu *et al.* (*27*), and although they suggested plausible routes to higher-oxygenated products ($O > 5$), the HOM formation hypothesis remains to be tested by systematic characterization of the HOM product distribution. In addition, HOM products from α-pinene + OH were mainly determined at very short reaction times [e.g., 3 to 7.9 s by Berndt *et al.* (*26*)], and therefore, products

[1]Department of Atmospheric and Oceanic Sciences & Institute of Atmospheric Sciences, Fudan University, Shanghai 200438, China. [2]Institute of Energy and Climate Research, IEK-8: Troposphere, Forschungszentrum Jülich GmbH, 52425 Jülich, Germany. [3]Physikalisches Institut, Universität zu Köln, 50932 Köln, Germany. [4]Shanghai Frontiers Science Center of Atmosphere-Ocean Interaction, Fudan University, Shanghai 200438, China. [5]Institute of Eco-Chongming (IEC), 20 Cuiniao Rd., Chongming, Shanghai 202162, China. [6]IRDR ICoE on Risk Interconnectivity and Governance on Weather/Climate Extremes Impact and Public Health, Fudan University, Shanghai 200438, China.
*Corresponding author. Email: dfzhao@fudan.edu.cn
†Present address: Department of Applied Physics, University of Eastern Finland, Kuopio, 70210, Finland.

formed via fast sequences of bimolecular peroxy radical steps at the time scale of several tens to hundreds of seconds may still be missing. Thus, HOM formation in the ambient atmosphere, where the RO_2• lifetimes can be long (up to several hundreds of seconds) (*31*, *32*), may involve alternative OH-initiated pathways. To our knowledge, systematic characterization of the HOM composition formed in the α-pinene oxidation by OH on a time scale of several minutes has not been reported and the underlying chemistry remains unexplored.

In this study, we investigated the OH-initiated oxidation of α-pinene under atmospherically relevant conditions in the outdoor SAPHIR chamber (Simulation of Atmospheric PHotochemistry In a large Reaction chamber) in experiments designed to minimize the impact of HOM production from ozonolysis reactions as demonstrated by direct OH radical and ozone measurements. We characterized the HOM composition in experiments at both low-NO [30 to ~100 parts per trillion (ppt)] and high-NO [~20 parts per billion (ppb)] mixing ratios representative for remote environments and areas influenced by anthropogenic activities, respectively. We further calculated the loss rates of different reaction pathways of peroxy radicals, the key intermediates in HOM formation, using measured HO_2•, RO_2•, and NO_X concentrations. Unexpectedly, more than 70% of C_{10}-HOM from α-pinene + OH were related to $C_{10}H_{15}O_X$• peroxy radicals in both low- and high-NO experiments in this study. We attribute these $C_{10}H_{15}O_X$•-related C_{10}-HOMs to be formed from the hydrogen abstraction pathway by OH rather than from the previously suggested addition pathway of OH as the first step in the oxidation of α-pinene by OH. We propose a plausible pathway of OH-initiated HOM formation, which is supported by theoretic kinetics calculations. H-abstraction pathways have been proposed for monoterpenes (*28*, *33*–*36*) contributing typically about 10% to oxidation by OH; therefore, they are usually not included in atmospheric chemical models as being of minor interest.

RESULTS

HOM product distribution

In the chamber experiments of OH oxidation of α-pinene, a $C_{10}H_{15}O_X$•-related HOM chemistry, including both peroxy radicals and their related termination products, dominated over the expected $C_{10}H_{17}O_X$•-related chemistry at both low NO (NO: 30 to ~100 ppt; Fig. 1A) and high NO (NO: ~20 ppb; Fig. 1B). On the basis of the established HOM chemistry (*18*, *37*), $C_{10}H_{15}O_X$• peroxy radicals are expected to be terminated by self-OH elimination or reactions with other RO_2•, NO, or HO_2• to form C_{10} closed-shell products with 14 H-atoms (likely carbonyls), 15-H-atoms (organic nitrates), or 16 H-atoms (alcohols and hydroperoxides) as shown in Fig. 1E and fig. S2. On the basis of the measured concentrations of RO_2•, HO_2•,

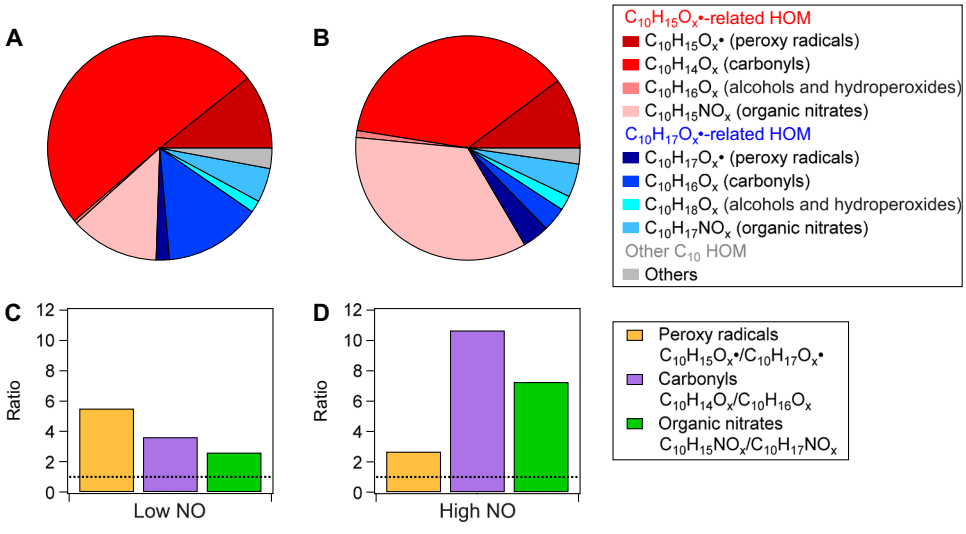

E

RO_2•	Unimolecular termination	RO_2• + RO_2•	RO_2• + HO_2•	RO_2• + NO
$C_{10}H_{15}O_x$•	$C_{10}H_{14}O_{x-1}$ (carbonyl)	$C_{10}H_{14}O_{x-1}$ (carbonyl) $C_{10}H_{16}O_{x-1}$ (alcohol)	$C_{10}H_{16}O_x$ (hyroperoxide)	$C_{10}H_{15}NO_{x+1}$ (organic nitrate)
$C_{10}H_{17}O_x$•	$C_{10}H_{16}O_{x-1}$ (carbonyl)	$C_{10}H_{16}O_{x-1}$ (carbonyl) $C_{10}H_{18}O_{x-1}$ (alcohol)	$C_{10}H_{18}O_x$ (hydroperoxide)	$C_{10}H_{17}NO_{x+1}$ (organic nitrate)

Fig. 1. C_{10}-HOM from OH oxidation of α-pinene in low-NO (30 to ~100 ppt) and high-NO (~20 ppb) experiments. The distribution of $C_{10}H_{15}O_X$•-related HOM (red), $C_{10}H_{17}O_X$•-related HOM (blue), and other C_{10}-HOM (gray) from α-pinene + OH during the first 15-min reaction time in (**A**) low-NO and (**B**) high-NO experiments. Four families, including peroxy radicals, carbonyls, alcohols and hydroperoxides, and organic nitrates, were identified in both $C_{10}H_{15}O_X$•- and $C_{10}H_{17}O_X$•-related C_{10}-HOM. Concentration ratios of these $C_{10}H_{15}O_X$•- to $C_{10}H_{17}O_X$•-related families under (**C**) low NO and (**D**) high NO are denoted in bar charts, with peroxy radicals in yellow, carbonyls in purple, and organic nitrates in green. Note that concentrations of the family of alcohols and hydroperoxides in both $C_{10}H_{15}O_X$•- and $C_{10}H_{17}O_X$•-related HOM are negligible and are thus not shown in the figure. The horizontal dashed lines in the bar charts represent equal contribution (ratio 1). The details of determining the ratio of $C_{10}H_{15}O_X$•-related to $C_{10}H_{17}O_X$•-related carbonyl are provided in section S3. (**E**) Possible reactions leading to C_{10} closed-shell products (carbonyls, organic nitrates, and alcohols and hydroperoxides) are listed for individual peroxy radicals, including $C_{10}H_{15}O_X$• (red) and $C_{10}H_{17}O_X$• (blue).

and NO, an average bimolecular RO_2• loss rate of ~0.02 s^{-1} (low NO) and ~ 3.5 s^{-1} (high NO) predominately due to the reaction with NO was estimated in our previous study (*38*). The expected main C_{10} closed-shell product families of $C_{10}H_{15}O_X$• (X = 6 to 14) are the carbonyls $C_{10}H_{14}O_X$ (X = 6 to 16) and organic nitrates $C_{10}H_{15}NO_X$ (X = 6 to 15; Fig. 1A). Analogously, $C_{10}H_{17}O_X$• (X = 7 to 14) forms the carbonyl family with formulas $C_{10}H_{16}O_X$ (X = 6 to 16) and the organic nitrate family $C_{10}H_{17}NO_X$ (X = 6 to 14; Fig. 1B). Note that in the following text, "X" will be used as defined here when one product family is referred to. The relative abundances of each individual product are shown in fig. S6. Other possible C_{10} closed-shell products of $C_{10}H_{15}O_X$• and $C_{10}H_{17}O_X$• are listed in Fig. 1E. Note that products with formulas $C_{10}H_{16}O_X$ can arise either from $C_{10}H_{15}O_X$• peroxy radicals as alcohols or hydroperoxides or from $C_{10}H_{17}O_X$• as carbonyls, while all other families can uniquely be attributed to one peroxy radical family. The separation of $C_{10}H_{15}O_X$• and $C_{10}H_{17}O_X$• chemistry's contributions to $C_{10}H_{16}O_X$ is discussed in section S3. During the early stage of the reaction time (0 to 15 min), the sum of peroxy radical concentrations of the $C_{10}H_{15}O_X$• family was more than twice as much as that of the $C_{10}H_{17}O_X$• family regardless of the NO concentration (Fig. 1, C and D). We also observed higher concentrations of C_{10} termination product families related to $C_{10}H_{15}O_X$• compared to $C_{10}H_{17}O_X$•. Concentrations of carbonyls ($C_{10}H_{14}O_X$) and organic nitrates ($C_{10}H_{15}NO_X$) stemming from $C_{10}H_{15}O_X$• radicals are 3.5 and 2.5 times higher than those of their counterparts $C_{10}H_{16}O_X$ and $C_{10}H_{17}NO_X$ from $C_{10}H_{17}O_X$• at low NO (Fig. 1C), and 10.7 and 6.9 times higher at high NO (Fig. 1D). Note that concentrations of alcohol and hydroperoxide products of $C_{10}H_{16}O_X$ and $C_{10}H_{18}O_X$ from respective reactions of $C_{10}H_{15}O_X$• and $C_{10}H_{17}O_X$• radicals are negligible. Both the predominant contribution of the $C_{10}H_{15}O_X$• peroxy radicals themselves and of the related $C_{10}H_{14}O_X$ and $C_{10}H_{15}NO_X$ HOM demonstrate the leading role of the $C_{10}H_{15}O_X$• peroxy family in the OH-induced HOM formation from α-pinene at low and high NO.

In this study, we assume that $C_{10}H_{15}O_X$•- and $C_{10}H_{17}O_X$•-related HOM have the same measurement sensitivity in NO_3^--CIMS. The rationale is that autoxidation provides two or more hydrogen bond donors (-OOH or -OH) in $C_{10}H_{15}O_X$•- and $C_{10}H_{17}O_X$•-related HOM with six and more oxygen atoms (*18*, *37*). These H bond donors allows HOMs to form strong clusters with NO_3^-, with rates near the collision limit similar to H_2SO_4 as they are able to compete with the very stable $(HNO_3)NO_3^-$, thus leading to the same high sensitivity (*39*). Moreover, the chemical structures of radicals, and carbonyls and organic nitrates with the same number of O atoms arising from $C_{10}H_{15}O_X$• or $C_{10}H_{17}O_X$•, only differ by one C=C bond or an endocyclic peroxide ring. Such differences are unlikely to substantially change the multiple H bonding–based sensitivity of NO_3^--CIMS to $C_{10}H_{15}O_X$•-related families and $C_{10}H_{17}O_X$•-related families (*40*). Experimentally, Pullinen *et al.* (*41*) used the same NO_3^--CIMS with the same setting and found no dependence of sensitivity on the functional groups of HOM, within a maximum uncertainty of a factor of 2. Therefore, we conclude that the sensitivity of NO_3^--CIMS to $C_{10}H_{15}O_X$•- and $C_{10}H_{17}O_X$•-related HOM is the same and near the collision limit. Applying the uncertainty factor of 2 to the $C_{10}H_{17}O_X$•-related families, concentration ratios became $C_{10}H_{14}O_X$•:$C_{10}H_{16}O_X$• = 1.8 (low NO) and 5.4 (high NO), and $C_{10}H_{15}NO_X$:$C_{10}H_{17}NO_X$ = 1.2 (low NO) and 3.5 (high NO). Even within this uncertainty, the role of $C_{10}H_{15}O_X$• chemistry remains important in the HOM formation from OH oxidation of α-pinene.

At low NO, a strong contribution of the $C_{10}H_{15}O_X$• family is also evident in the abundance of accretion products with 20 C-atoms (C_{20}-HOM). C_{20}-HOMs are formed via the self- and cross-reactions (*42*, *43*) of $C_{10}H_{15}O_X$• and $C_{10}H_{17}O_X$• peroxy radicals via the loss of two O-atoms. We observed C_{20}-HOM, with a concentration ratio for $C_{20}H_{30}O_X$ (X = 6, 9 to 17):$C_{20}H_{32}O_X$ (X = 9 to 17):$C_{20}H_{34}O_X$ (X = 10 to 14) of 1:2.2:1.6 within the first 15 min of the reaction of α-pinene + OH (fig. S9C). Considering the possible permutations, accretion products $C_{20}H_{30}O_{2n-2}$ and $C_{20}H_{34}O_{2n-2}$ are formed solely by $C_{10}H_{15}O_n$• or $C_{10}H_{17}O_n$•, respectively, while cross-reactions of $C_{10}H_{15}O_n$• and $C_{10}H_{17}O_n$• lead to $C_{20}H_{32}O_{2n-2}$. Note that the concentration ratios of HOM $C_{10}H_{15}O_X$• to $C_{10}H_{17}O_X$• need not exactly match the corresponding dimer ratios, $C_{20}H_{30}O_X$ to $C_{20}H_{34}O_X$, because less oxygenated $C_{10}H_{15}O_X$• to $C_{10}H_{17}O_X$• also participate in accretion reactions as shown in previous studies (*15*, *41*, *42*, *44*). The dominance of $C_{10}H_{15}O_X$• observed for HOM (X > 6) is not necessarily applicable to less oxygenated compounds, where indeed $C_{10}H_{17}O_X$• should dominate in OH oxidation of α-pinene. Therefore, observation and concentration ratios of $C_{20}H_{34}O_X$- and $C_{20}H_{32}O_X$-HOM here do not contradict our finding of the dominance of $C_{10}H_{15}O_X$•-related products in C_{10}-HOM. In contrast, the strong presence of the "mixed" $C_{20}H_{32}O_X$ family and the observation of the $C_{20}H_{30}O_X$ family underline the central role of the $C_{10}H_{15}O_X$• peroxy radicals. At high NO (fig. S4B), accretion products are negligible, because reactions with NO suppress their formation (*41*, *45*–*47*).

We also observed substantial fractions of C_7-HOM, which are expected to arise from bond scission reactions of alkoxy radicals. We attribute their origin to the $C_{10}H_{15}O_X$• and $C_{10}H_{17}O_X$• families with details being discussed in section S6. The strong C_7-HOM product formation and the dominance of $C_7H_9O_X$• (originating from $C_{10}H_{15}O_X$• peroxy radicals)–related products over $C_7H_{11}O_X$• (originating from $C_{10}H_{17}O_X$• peroxy radicals)–related products are also in support of the dominance of a $C_{10}H_{15}O_X$• peroxy radical chemistry, as well as indicative of the importance of pathways involving alkoxy radicals. As we will show in the following, alkoxy radicals play a central role in OH-induced pathways to $C_{10}H_{15}O_X$• peroxy radicals from α-pinene.

OH-induced pathways to $C_{10}H_{15}O_x$•

Addition of OH to the double bond of α-pinene ($C_{10}H_{16}$) is its accepted major oxidation pathway [~90%; (*26*, *48*)] and results in peroxy radicals $C_{10}H_{17}O_3$• with 17 H-atoms. Subsequent autoxidation leads to peroxy radicals with formulas $C_{10}H_{17}O_X$• (fig. S12A). This is not compatible with our observations on 15-min time scales. We propose that the pathway of hydrogen abstraction by OH forms $C_{10}H_{15}O_2$• after O_2 addition (*28*, *29*), a peroxy radical that has 15 H-atoms like the observed HOM. $C_{10}H_{15}O_2$• is then the starting point for forming the $C_{10}H_{15}O_X$• peroxy radical family by autoxidation steps.

An alternative pathway forming $C_{10}H_{15}O_X$• peroxy radicals can start from a first-generation C_{10} oxidation products in α-pinene + OH reaction. We consider pinonaldehyde ($C_{10}H_{16}O_2$) (*34*) as the most competitive candidate, which is one of the main products in α-pinene + OH reaction and the most abundant first-generation C_{10} product reported (fig. S12, B and C). H-abstraction by OH and subsequent O_2 addition leads to $C_{10}H_{15}O_4$•, which could also be a starting point to form the $C_{10}H_{15}O_X$• family by further autoxidation steps. However, on the 15-min time scale of our experiments, the pinonaldehyde product has not yet accumulated and the rate of the H-abstraction reaction from α-pinene by OH is much faster compared

to pinonaldehyde (at least 70 and 8 times faster at low and high NO, respectively; see section S7). As pinonaldehyde is the most abundant first-generation C_{10} product and reacts fast with OH (3.9×10^{-11} cm^3 $molecule^{-1}$ s^{-1} at 298 K), other C_{10} first-generation products are expected to be even less important in forming $C_{10}H_{15}O_X$• because of lower yield and reactivity, or the inability to produce $C_{10}H_{15}O_X$• when reacting with OH, such as C_{10}-hydroxynitrate. Therefore, we conclude that direct hydrogen abstraction by OH from α-pinene is the responsible pathway to $C_{10}H_{15}O_X$• peroxy radicals in this study.

The most likely routes to form $C_{10}H_{15}O_2$• peroxy radicals subsequent to the hydrogen abstraction from α-pinene by OH shown in Fig. 2 are based on calculated rate constants (*28*). The initial hydrogen abstraction is expected to occur on C4, leading to an allylic radical with two resonance radical sites, R1 and R2, which immediately react with O_2 forming the peroxy radicals R1OO and R2OO with an estimated ratio of 40:60. These RO_2• have no competitive unimolecular reaction channels (table S1 and section S9). Under the experimental conditions with the presence of NO, R1OO and R2OO thus mainly undergo reactions with NO (as shown in fig. S7) and form the alkoxy radicals R1O and R2O (and organic nitrates, not shown in the Fig. 2). In the following, we denote the conversion of RO_2• to alkoxy radicals (RO•) by NO (RO_2• + NO ➔ RO• + NO_2) as an "alkoxy step." For R1O, the opening of the six-membered ring followed by O_2 addition leads to R3OO, which is unlikely to proceed to autoxidation because of the remaining four-membered ring (table S2 and section S10). However, peroxy radicals formed after one further alkoxy step, followed by ring cleavage and O_2 addition, are expected to easily undergo autoxidation (e.g., R6OO; fig. S18A). The competing 1,8 H-shift of the aldehydic H-atom in R3OO followed by one more alkoxy step can also lead to a peroxy radical, R9OO, which likewise can undergo fast autoxidation steps as shown in fig. S18B. Depending on the stereo-specific chemistry of the alkoxy radicals R2O (see fig. S15 and section S10), these will either undergo direct opening of the six-membered ring and form the peroxy radical R4OO while retaining the four-membered ring [about 60% (*28*)] or undergo 1,5 H-shift and subsequent cleavage of the four-membered ring R5OO (about 40%). According to our calculations, R4OO and R5OO have no viable unimolecular reactions to further react via an autoxidation step (table S2). Again, one more alkoxy step allows the opening of the remaining four- or six-membered ring in R4O and R5O with subsequent O_2 addition (Fig. 2) to proceed to autoxidation via R10OO and R11OO (see Fig. 2, and subsequent chemistry in fig. S18, C and D). R10OO and R11OO are predicted to react further with high-rate coefficients, for example, 8.7×10^2 s^{-1} for the five-membered ring closure of R10OO and 4×10^3 s^{-1} for the 1,8 H-shift of R11OO derived from structure-activity relationship (SAR), as described in section S11. This is related to the functionalization of R10OO and R11OO by the double bond (*49*) and the aldehyde group (*50*).

As shown in Fig. 2, alkoxy steps allow for the formation of RO•, which will undergo ring opening by α-scission at very fast rates. Ring opening, especially of the bicyclic frame of α-pinene and ultimately of both rings, is required to remove geometric strain in the molecule. Once migratable H-atoms are accessible, multistep autoxidation reactions lead to the formation of the $C_{10}H_{15}O_X$• peroxy radical family. In this study, RO• are mainly formed by the alkoxy step (RO_2• + NO ➔ RO• + NO_2), whose reaction rate depends on the current NO concentration, while the ring opening is especially fast with a typical rate $>10^6$ s^{-1} (*51*). As a consequence, the formation rate of $C_{10}H_{15}O_X$•-related HOM is mainly affected by the NO concentration. In our low-NO experiments, NO needed first to be formed by photolysis of HONO originating from the chamber walls (*52*). Note that the NO concentration increased gradually during the experiment at low NO (fig. S3A). The formation of $C_{10}H_{15}O_X$•-related products was consequently delayed by 3 to 4 min (Fig. 3A) because of the lack of fast RO• production from alkoxy steps at low NO concentration (30 to 50 ppt within the first 5-min reaction time). As the experiment proceeded, increasing NO accelerated the RO• production and the subsequent formation of $C_{10}H_{15}O_X$•-related carbonyls $C_{10}H_{14}O_X$ (Fig. 3A) and organic nitrates $C_{10}H_{15}NO_X$ (Fig. 3B). In the high-NO experiment, with NO concentrations of ~20 ppb (RO_2• lifetime of ~0.2 s), $C_{10}H_{15}O_X$•-related carbonyls and nitrates form immediately (<1 to 2 min; Fig. 3, C and D) because high concentrations of NO directly enabled the alkoxy steps. A similar time series pattern, i.e., 3 to 4 min delay at low NO and quick formation at high NO, was also observed in individual $C_{10}H_{15}O_X$•-related C_{10}-HOM, with several examples shown in fig. S8. Time series of both lumped and individual $C_{10}H_{15}O_X$•-related C_{10}-HOM are consistent with the role of NO in their formation and further support the proposed mechanism in Fig. 2, with rapid autoxidation after two alkoxy steps. At low NO, the autoxidation process of $C_{10}H_{17}O_X$• is competitive with bimolecular reactions with NO, with rapid H shifts (>0.1 s^{-1}) proposed in Xu *et al.* (*27*). Because the formation rate of $C_{10}H_{17}O_X$• peroxy radicals is independent of NO (*25*–*27*), time series of $C_{10}H_{17}O_X$•-related C_{10}-HOM are similar at low and high NO, with no delay at low NO observed, as shown in blue lines in Fig. 3 and fig. S8 (G to L). Increasing concentration ratios of $C_{10}H_{15}O_X$•-related C_{10}-HOM to $C_{10}H_{17}O_X$•-related C_{10}-HOM (Fig. 3, A and B) at low NO further support an accelerated $C_{10}H_{15}O_X$• chemistry by increasing NO as the reaction proceeds and a $C_{10}H_{17}O_X$• chemistry independent of NO, likely due to the absence of double bond (*53*) and aldehyde groups (*50*) compared to $C_{10}H_{15}O_X$•. At high NO, concentration ratios of $C_{10}H_{15}O_X$•-related C_{10}-HOM to $C_{10}H_{17}O_X$•-related C_{10}-HOM (Fig. 3, C and D) quickly reached a relatively stable value, where high NO concentrations allow rapid alkoxy steps and make $C_{10}H_{15}O_X$• chemistry dominant during the first 15-min reaction time. Moreover, concentration ratios of $C_{10}H_{15}O_X$•-related C_{10}-HOM over $C_{10}H_{17}O_X$•-related C_{10}-HOM are higher at high NO (~10) than at low NO (~2), also indicating the important role of NO in the formation of $C_{10}H_{15}O_X$•-related C_{10}-HOM from OH oxidation of α-pinene. The observed time series of $C_{10}H_{15}O_X$•-related C_{10}-HOM to $C_{10}H_{17}O_X$•-related C_{10}-HOM in Fig. 3 are generally similar to modeled results (fig. S22) after adding $C_{10}H_{17}O_X$• chemistry (*27*) to MCM (Master Chemical Mechanism). Detailed descriptions are given in section S12; briefly, we followed $C_{10}H_{17}O_X$• chemistry by Xu *et al.* (*27*) and incorporated full reactions leading to highly oxygenated products (O > 6) into our MCM calculations. For missing branching ratio and rate coefficients, uniform values were applied according to empirical knowledge from literature (*50*, *54*–*56*). Although the modeled concentration ratios of $C_{10}H_{15}O_X$•-related HOM to $C_{10}H_{17}O_X$•-related HOM match the trend of the observed ones well, they did not exactly reproduce the time scale of the initial increase at high NO (Fig. 3 and fig. S22). This may be attributed to the fact that the $C_{10}H_{15}O_X$• HOM chemistry proposed in this study is still not complete, as only the most likely formation pathways were included, and some important pathways may be missing, particularly alkoxy-peroxy pathways for highly oxygenated RO_2• (O > 6). Similarly, $C_{10}H_{17}O_X$• HOM chemistry included in our MCM model study

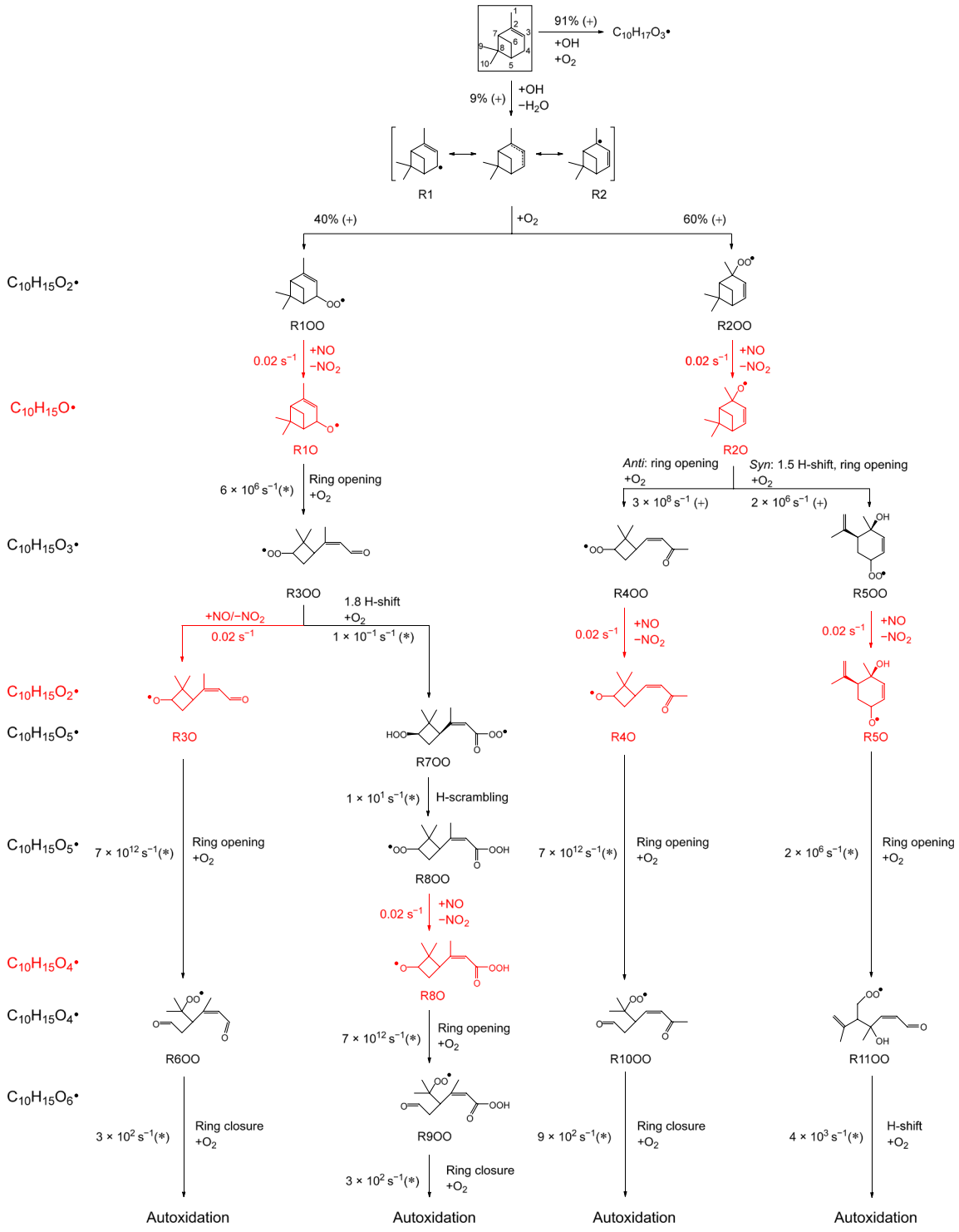

Fig. 2. Formation pathways to $C_{10}H_{15}O_X$• radicals and their structures. Simplified reaction scheme at 298 K after H-abstraction from α-pinene (shown in the box) by OH leading to $C_{10}H_{15}O_X$• radicals that can undergo further autoxidation. Only pathways leading to HOM formation are included in this figure; other competing pathways are described in sections S9 and S10. Alkoxy steps are highlighted in red. Alkyl radicals are labeled as R#, while alkoxy radicals and peroxy radicals are labeled as R#O and R#OO. Chemical formulas are denoted on the left side of the figure. Rate of alkoxy radical formation in the RO_2• + NO reactions is estimated on the basis of 100 ppt of NO and an organic nitrate yield of 0.1. Unimolecular rate coefficients are derived from structure-activity relationships (SARs) (*) or taken from Peeters *et al.* (*28*) (+). See the Supplementary Materials for more detailed stereo-specific chemistry, further autoxidation steps, and minor reactions with rates derived from SARs or explicit theoretical calculations.

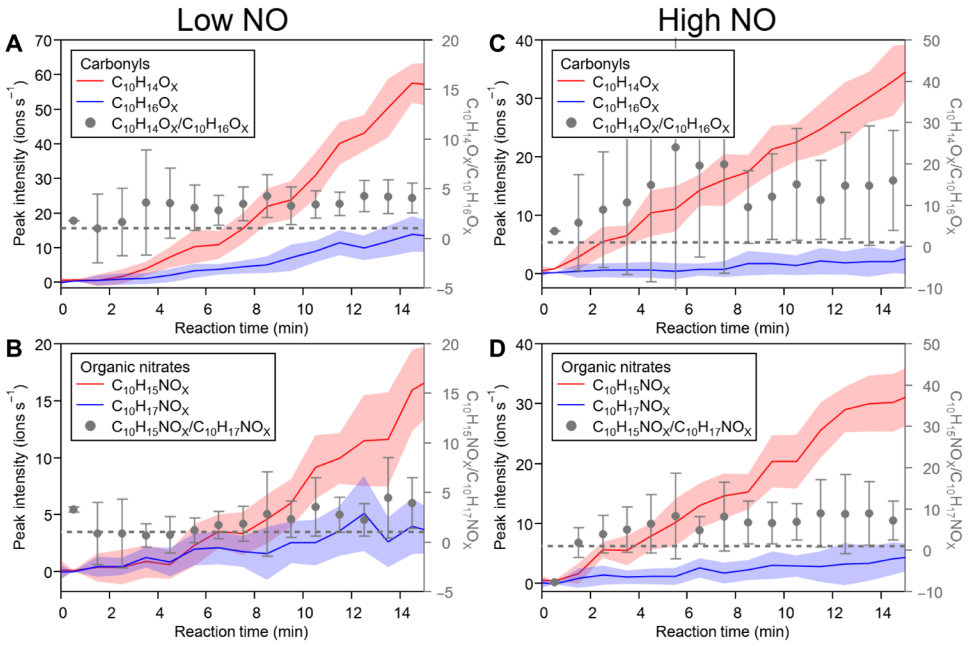

Fig. 3. Time series of $C_{10}H_{15}O_X$•- and $C_{10}H_{17}O_X$•-related families of carbonyls and organic nitrates in low-NO (30 to ~100 ppt) and high-NO (~20 ppb) experiments. For the carbonyl family, $C_{10}H_{14}O_X$ (red), $C_{10}H_{16}O_X$ (blue), and their concentration ratio ($C_{10}H_{14}O_X$ to $C_{10}H_{16}O_X$, gray) during the first 15-min reaction are shown in (**A**) low-NO and (**C**) high-NO experiments. Time series of the family of organic nitrates, including $C_{10}H_{15}NO_X$ (red), $C_{10}H_{17}NO_X$ (blue), and concentration ratio of $C_{10}H_{15}NO_X$ to $C_{10}H_{17}NO_X$, are similarly demonstrated in (**B**) low-NO and (**D**) high-NO experiments. The horizontal dashed lines represent a concentration ratio of 1, where $C_{10}H_{15}O_X$• chemistry is equal to $C_{10}H_{17}O_X$• chemistry. All data are averaged to a time resolution of 1 min. In each panel, error bars of $C_{10}H_{15}O_X$•- and $C_{10}H_{17}O_X$•-related products (left axes) represent 1 SD and error bars of concentration ratios (right axes) were calculated using error propagation.

is also not complete, as many rate constants are not available in the literature. Similar patterns to C_{10}-HOM were observed for the time series of C_7-HOM at both low and high NO, which is discussed in detail in the Supplementary Materials (section S6). In all cases, $C_{10}H_{15}O_X$•-related products became dominant over $C_{10}H_{17}O_X$•-related products after 3 to 4 min or 1 to 2 min at low and high NO, respectively (Fig. 3 and fig. S11), underlining the importance of the $C_{10}H_{15}O_X$• peroxy radical family for HOM formation.

Compared to the pathways involving the $C_{10}H_{17}O_X$• peroxy radical family (*25*–*27*), our mechanism for the OH-induced formation of the $C_{10}H_{15}O_X$• peroxy radical family includes the minor H-abstraction channel as a rate-limiting step as well as a minimum of two bimolecular reaction steps. The question arises whether the bimolecular reaction steps are sufficiently fast to explain the observed HOM formation. We applied the mechanism presented in Fig. 2 in model calculations using explicit reaction rate constants for the individual peroxy radicals and calculated the time evolution of $C_{10}H_{15}NO_9$ as an example (see details in section S12). It appeared that our mechanism indeed explains the observed $C_{10}H_{15}NO_9$ concentrations in both the low- and high-NO experiments (fig. S19 and section S12). The calculations reproduce the delay period in the low-NO experiment and the accelerated $C_{10}H_{15}NO_9$ formation at high NO. The delayed formation time at low NO is indeed related to the alkoxy production rate as shown in fig. S20. The sensitivity of the model results to the model parameters is also discussed in more detail in the Supplementary Materials.

We conclude that the H-abstraction channel with subsequent alkoxy steps is sufficient to explain an OH-induced $C_{10}H_{15}O_X$•-related HOM chemistry on minute time scales. We further conclude that OH-induced HOM formation (from α-pinene) must be preceded by the formation and intramolecular rearrangements of alkoxy radicals to open the ring structures and thereby enabling intramolecular H-shifts in peroxy radicals (autoxidation steps).

The formation of the $C_{10}H_{15}O_X$• peroxy radical family and the uniquely related HOM families $C_{10}H_{14}O_X$ and $C_{10}H_{15}NO_X$ have been reported before in α-pinene + OH experiments. A dominance of a $C_{10}H_{15}O_X$•-based over a $C_{10}H_{17}O_X$•-based chemistry was also observed by Kang (*57*) and Pullinen *et al.* (*41*) at low and high NO_X, although the HOM chemistry may differ as their experiments contained O_3 and were conducted in the continuous stirred tank reactor JPAC under steady-state conditions with typical reaction times of several tens of minutes. In the same sense, Yan *et al.* (*46*) observed similar $C_{10}H_{15}O_X$•-related products in the CLOUD chamber, including $C_7H_8O_X$ and $C_7H_9NO_X$ and accretion products $C_{20}H_{30}O_X$ and $C_{20}H_{32}O_X$, although the contribution of ozonolysis of α-pinene to the formation of these compounds cannot be ruled out. Other laboratory studies (*25*–*27*) on HOM from α-pinene + OH reported only the formation of $C_{10}H_{17}O_X$•-related products. The missing $C_{10}H_{15}O_X$• products may be attributed to the different experimental conditions. For example, at very short reaction times of 2.6 to 7.9 s (*25*, *26*), the importance of alkoxy formation from bimolecular reactions may be reduced (with an estimated bimolecular RO_2• lifetime of 1.7 min at low NO), and the OH addition channel dominates the HOM formation via $C_{10}H_{17}O_X$• peroxy radicals. This is not in contradiction to our study, where also in the first 1 to 2 min at low NO, $C_{10}H_{17}O_X$•-based products are most abundant, consistent with the findings of Berndt *et al.* (*26*). Varying the concentrations of NO, Berndt (*25*) still only observed $C_{10}H_{17}O_{3-7}$• using $C_2H_5NH_3^+$

and I^- reagent ions. While the reason for the absence of $C_{10}H_{15}O_X$• and $C_{10}H_{17}O_{>7}$• is not completely clear, there may be two possible reasons. First, the concentrations of $C_{10}H_{15}O_X$•-related C_{10}-HOM may be relatively low, particularly $C_{10}H_{15}O_{<8}$• (fig. S6) due to fast H shifts and the reaction time (7.5 s) in the experiments of Berndt (*25*). This is consistent with the likely dominant role of $C_{10}H_{17}O_X$• chemistry in the low oxygenated molecules (O < 6) from OH addition channel but the important $C_{10}H_{15}O_X$• chemistry in the formation of HOM with six and more oxygen atoms. In addition, the peaks of $C_{10}H_{15}O_X$• in mass spectra are very close to $C_{10}H_{17}NO_X$ (differing by 0.024 Th), which may be thus covered in the peaks of $C_{10}H_{17}NO_X$. Second, although $C_2H_5NH_3^+$ ionization is generally sensitive to detect oxygenated compounds with a wide range of oxygenation, it may not be sensitive to every HOM as shown for products in the reaction of isoprene with OH (*58*). I^- ionization has been shown to be not sensitive to more oxygenated organics (*59*). As discussed above, it is unlikely that the same ionization scheme [here, NO_3^- reagent ions in an Eisele type inlet (*39*, *40*, *60*, *61*)] biases $C_{10}H_{15}O_X$•-related over $C_{10}H_{17}O_X$•-related compounds as both families should carry similar functional groups (for the same number of O-atoms) despite the different number of H-atoms.

Last, HOM products based on the $C_{10}H_{15}O_X$• family have been observed in the reaction of α-pinene with Cl•-atoms, which has a stronger preference to abstract a hydrogen atom from α-pinene compared to OH (*62*). Recent α-pinene + Cl• laboratory studies have found monomers of the $C_{10}H_{14}O_X$ family and $C_{20}H_{30}O_X$ accretion products as main HOM products and attributed those to the hydrogen abstraction channel. However, the site specificity is still unknown (*63*, *64*). This finding provides strong support that HOM can be formed indeed from a hydrogen abstraction channel of α-pinene.

HOM molar yields of OH induced $C_{10}H_{15}O_X$•-related formation pathways

The $C_{10}H_{15}O_X$•-related HOM molar yields from OH oxidation of α-pinene were estimated to be 0.8% (−0.4%/+1.2%) at low NO and 0.7% (−0.4%/+1.0%) at high NO, accounting for about 70 and 82% of the total HOM yield, respectively. The total HOM yield, 1.1% (−0.6%/+1.6%) at low NO and 0.8% (−0.4%/+1.2%) at high NO, is roughly within the range of reported values 0.05 to 1.5% [based on the measurements with a nitrate CIMS (*11*, *12*, *21*, *26*) in table S5], although the chemistry may differ in these different experiments. This yield is lower than the HOM yield measured using acetate and ethylaminium ionization schemes (table S5) (*25*, *26*, *65*). The yields were calculated for the first 15-min reaction time and include wall loss and dilution corrections (see details in Materials and Methods). Note that the HOM yields here using the calibration coefficient derived from H_2SO_4 (*58*) represent lower limit values with an uncertainty of a factor of ~2. The slightly lower molar yields at high NO concentrations may be attributed to fast alkoxy fragmentation processes leading to small molecules (*51*), which can only be measured with limited sensitivity by the nitrate CIMS instrument (*39*, *40*).

DISCUSSION

Our study provides clear evidence that the hydrogen abstraction channel in the α-pinene + OH reaction dominates the HOM formation via $C_{10}H_{15}O_X$• on time scales of several minutes, at both low-NO (30 to ~100 ppt) and high-NO (~20 ppb) mixing ratios. This indicates that the HOM formation takes another route other than the major route via the OH addition channels (e.g., MCM v.3.1.1). HOM formation initiated by H-abstraction by OH radicals can explain the HOM product distribution found in the ambient atmosphere in previous studies. For example, on the basis of the source apportionment analysis of time-resolved HOM mass spectra, Yan *et al.* (*66*) isolated a daytime factor containing $C_{10}H_{15}NO_8$ as the major peak in Hyytiälä, a forest site in north Finland. This was supposed to be controlled by OH oxidation of monoterpenes although some contribution of ozonolysis could not be excluded. Jokinen *et al.* (*67*) suggest photochemical production pathways involving the OH oxidation for $C_{10}H_{15}NO_8$ and $C_{10}H_{15}NO_9$ in Hyytiälä because of their considerable decreased concentrations during a solar eclipse. Field results (*68*) from the Southern Oxidant and Aerosol Study campaign showed a main peak concentration of $C_{10}H_{15}NO_{7-11}$ after sunrise when the concentrations of NO were high and O_3 concentrations were low, with an estimated $C_{10}H_{17}NO_{6-9}$–to–$C_{10}H_{15}NO_{7-11}$ concentration ratio of ~1:2. If these products were formed by the OH addition as previously thought, the major peak should be $C_{10}H_{17}NO_{6-9}$ rather than $C_{10}H_{15}NO_{7-11}$.

HOM from hydrogen abstraction by OH can be an important source of HOM in areas with high monoterpene emission rates. Pye *et al.* (*69*) found that OH dominates monoterpene loss rates in many regions such as Europe, a large part of the United States, and China [fig. S9D in the Supporting Information (*69*)]. The HOM production rate by OH via the hydrogen abstraction channel could reach up to 25 to 30% of the total $C_{10}H_{15}O_X$•-related HOM production rate by OH and O_3, calculated by using average concentrations of 2×10^6 and 7×10^{11} molecule cm^{-3} for OH and O_3 (*70*) and respective molar yields of 0.7 to 0.8% for OH-induced HOM (this study) and 2.9 to 3.4% for O_3-induced HOM (*12*, *21*). In regions with high OH concentrations of up to 1.5×10^7 cm^{-3} such as Southern China (*71*), isomerization reactions of alkoxy radicals from the hydrogen abstraction channel can contribute to 71 to 76% of the production rate of the $C_{10}H_{15}O_X$•-related HOM from both OH and O_3. Hence, the OH oxidation pathway via the hydrogen abstraction channel is not negligible in the formation of HOM; in particular, highly oxygenated organic nitrates of the $C_{10}H_{15}NO_X$ family were observed in the above field studies (*66*, *68*) and may play a potentially competitive or even dominant role in the OH-rich atmosphere. The hydrogen abstraction by OH may also be important for HOM formation from other monoterpenes (*35*, *72*) as well as from other unsaturated VOCs if ring opening is a key prerequisite.

Because HOM can account for a substantial mass fraction of SOA, especially in the early growth of particles in new particle formation events, the hydrogen abstraction channel should be taken into account in numerical models to accurately simulate HOM and SOA concentrations and predict new particle formation and SOA growth, particularly in OH-rich areas (*69*), such as the Southeastern United States and Southern China. However, current chemical mechanisms, such as α-pinene + OH reactions in MCM v3.1.1, ignore the hydrogen abstraction channel and typically only include OH addition pathways, leading to $C_{10}H_{17}O_X$•-related first-generation products as mentioned above. This simplification is mainly due to the low branching ratio (~10%) of hydrogen abstraction compared to that of the OH addition channel (90%) (*29*). Our study indicates that a minor initial reaction pathway can be an important or even dominant pathway for selected processes like HOM formation. Through HOM, the minor H-abstraction channel unexpectedly

gains in importance for processes related to submicrometer aerosols, like new particle formation and SOA growth, with consequences for all kinds of impacts of submicrometer aerosols, e.g., activation of cloud condensation nuclei and, thus, climatic impact of aerosols.

Our study also highlights the role of alkoxy radicals in HOM formation besides autoxidation. As NO_X is ubiquitous in the ambient atmosphere, forming alkoxy radicals is common as RO_2• + NO is expected to be a dominant loss path of peroxy radicals in urban areas and in most of the remote regions on the continent because of the wide influence of anthropogenic emissions on the planet except for very remote areas such as Amazonia over certain seasons. In addition, other reactions of RO_2• such as with RO_2• or HO_2• may also form alkoxy radicals. Because of their fast unimolecular reactions such as ring opening, alkoxy steps can facilitate fast autoxidation forming HOM that would be otherwise not possible (*73*). The role of alkoxy radical in HOM formation in other reaction systems (*74*) such as for other VOCs and other oxidants, and in the ambient atmosphere, warrants further studies.

MATERIALS AND METHODS

Experimental procedure and instrumental setup

The experiments were conducted in the SAPHIR chamber (August 2013) (*75*) under representative environmental conditions of low NO (30 to ~100 ppt) and high NO (~20 ppb) concentrations. Note that the "low" and "high" designators here are solely used to distinguish the NO concentrations in these two types of experiments, as RO_2• will mainly react with NO in both cases. Details of the RO_2• fate in our study are explicitly derived from measured RO_2•, HO_2•, and NO concentrations. The details of the experiments have been described previously (*38*). We started our experiments by humidifying the air in the dark chamber to ~75% relative humidity and then the precursor α-pinene (~20 ppb) was added. In the low-NO experiment, no NO was added and the NO in the SAPHIR chamber arises from the photolysis of HONO produced via a well-characterized photolytic source related to the Teflon wall. The source strength is a function of relative humidity and the solar radiation (*52*). In the case of the high-NO experiment, additional NO (~20 ppb) was injected. Then, the shutter system of the roof was opened to start photooxidation of α-pinene using sunlight. In both low- and high-NO experiments, OH radicals were generated from the photolysis of HONO (*52*). No O_3 was added in either of the experiments. During the early-stage reaction period (0 to 15 min), on which the focus is in this study, mixing ratios of O_3 remained below the detection limit of 1 ppb (fig. S3) and photo-oxidation reactions were ensured in both low- and high-NO experiments.

A $^{15}NO_3^-$ chemical ionization mass spectrometer (Aerodyne Research Inc., USA) was used to detect gaseous HOM, particularly products with six or more oxygen atoms (*39*, *40*, *60*, *61*). Nitrogen-15 was used to distinguish reagent ion nitrogen from the nitrogen-14 atoms in the chamber-produced organic nitrates. The mass spectra within the mass range of *m/z* (mass/charge ratio) 4 to 1400 were analyzed using the Tofware analysis toolkit (Tofwerk/Aerodyne) in Igor Pro (WaveMetrics Inc.). High-resolution analysis was applied to identify ions with a resolving power $m/z/\Delta m/z$ of ~3000, with example fitting results shown in fig. S5. Other instruments used to characterize both gas- and particle-phase species are described in detail in section S2.

$C_{10}H_{15}O_X$•-related HOM molar yield quantification

According to the definition in Bianchi *et al.* (*18*), HOMs were identified as organic compounds containing six or more O atoms and formed from the autoxidation pathway. As $C_{10}H_{15}O_X$•-related contributions to C_7, C_{10}, and C_{20} HOM could be identified, the contribution of $C_{10}H_{15}O_X$•-related HOM to the total HOM concentration was estimated by summing over these contributions. Note that detailed calculations to separate the contribution of $C_{10}H_{17}O_X$•-related carbonyl compounds to $C_{10}H_{16}O_X$ can be found in section S3, with similar kinetics of $C_{10}H_{15}O_X$• and $C_{10}H_{17}O_X$• assumed. A calibration coefficient (*C*) was used to convert the mass spectra signals of HOM to concentrations. The calibration coefficient was derived from calibrations with H_2SO_4, whose charge efficiency is assumed to be the same as for HOM. The details of the calibration with H_2SO_4 can be found in Zhao *et al.* (*76*) and Shen *et al.* (*44*). A value of 2.5×10^{10} molecule cm^{-3} nc^{-1} (nc = normalized counts) with an uncertainty of −52%/+143% was used in this study. Note that accretion products are formed from two monomer peroxy radicals, so that molar concentrations of accretion products were multiplied by 2. The molar yield of total HOM was calculated as below

$$Y = \frac{[\mathrm{HOM}_{C\leq 10}] + 2\times[\mathrm{HOM}_{C>10}]}{[\alpha\text{-pinene}]_{\mathrm{reacted}}} = \frac{(I(\mathrm{HOM}_{C\leq 10}) + 2\times I(\mathrm{HOM}_{C>10}))\times C}{[\alpha\text{-pinene}]_{\mathrm{reacted}}} \quad (1)$$

where [HOM] is the concentration of HOM, *I*(HOM) is peak intensity of HOM normalized to the total mass spectra signals, and $[\alpha\text{-pinene}]_{\mathrm{reacted}}$ is the concentration of α-pinene reacted. The concentrations of HOM were also corrected for wall loss using a wall loss rate of 6×10^{-4} s^{-1} (low NO) (*77*) and 2.2×10^{-3} s^{-1} (high NO), and a dilution rate of 1.5×10^{-5} s^{-1} (both low and high NO). The higher wall loss rate at high NO is due to running fans in the chamber. The uncertainty of HOM molar yields is estimated to be −55%/+144%, with details shown in section S4.

Theoretical kinetic predictions

The theoretical methodologies are described in detail in the Supplementary Materials. Briefly, quantum chemical calculations were performed at the CCSD(T)/aug-cc-pVTZ//M06-2X-D3/aug-cc-pVTZ level of theory for 30 reactions of RO_2• radicals formed in the α-pinene H-abstraction channel. These data are used to derive rate coefficients using multiconformer transition state theory with Eckart tunneling correction, accounting for all conformers of reactants and transition states. For the reactions of noncyclic RO_2• radicals and for alkoxy radicals in the oxidation scheme, no direct calculations were performed but rate coefficients were derived on the basis of SARs available in the literature; the procedure is described in detail in the Supplementary Materials.

SUPPLEMENTARY MATERIALS

Supplementary material for this article is available at https://science.org/doi/10.1126/sciadv.abp8702

REFERENCES AND NOTES

1. Q. Zhang, J. L. Jimenez, M. R. Canagaratna, J. D. Allan, H. Coe, I. Ulbrich, M. R. Alfarra, A. Takami, A. M. Middlebrook, Y. L. Sun, K. Dzepina, E. Dunlea, K. Docherty, P. F. DeCarlo, D. Salcedo, T. Onasch, J. T. Jayne, T. Miyoshi, A. Shimono, S. Hatakeyama, N. Takegawa, Y. Kondo, J. Schneider, F. Drewnick, S. Borrmann, S. Weimer, K. Demerjian, P. Williams, K. Bower, R. Bahreini, L. Cottrell, R. J. Griffin, J. Rautiainen, J. Y. Sun, Y. M. Zhang, D. R. Worsnop, Ubiquity and dominance of oxygenated species in organic aerosols

in anthropogenically-influenced Northern Hemisphere midlatitudes. *Geophys. Res. Lett.* **34**, L13801 (2007).
2. M. Kanakidou, J. H. Seinfeld, S. N. Pandis, I. Barnes, F. J. Dentener, M. C. Facchini, R. Van Dingenen, B. Ervens, A. Nenes, C. J. Nielsen, E. Swietlicki, J. P. Putaud, Y. Balkanski, S. Fuzzi, J. Horth, G. K. Moortgat, R. Winterhalter, C. E. L. Myhre, K. Tsigaridis, E. Vignati, E. G. Stephanou, J. Wilson, Organic aerosol and global climate modelling: A review. *Atmos. Chem. Phys.* **5**, 1053–1123 (2005).
3. J. L. Jimenez, M. R. Canagaratna, N. M. Donahue, A. S. H. Prevot, Q. Zhang, J. H. Kroll, P. F. DeCarlo, J. D. Allan, H. Coe, N. L. Ng, A. C. Aiken, K. S. Docherty, I. M. Ulbrich, A. P. Grieshop, A. L. Robinson, J. Duplissy, J. D. Smith, K. R. Wilson, V. A. Lanz, C. Hueglin, Y. L. Sun, J. Tian, A. Laaksonen, T. Raatikainen, J. Rautiainen, P. Vaattovaara, M. Ehn, M. Kulmala, J. M. Tomlinson, D. R. Collins, M. J. Cubison, E. J. Dunlea, J. A. Huffman, T. B. Onasch, M. R. Alfarra, P. I. Williams, K. Bower, Y. Kondo, J. Schneider, F. Drewnick, S. Borrmann, S. Weimer, K. Demerjian, D. Salcedo, L. Cottrell, R. Griffin, A. Takami, T. Miyoshi, S. Hatakeyama, A. Shimono, J. Y. Sun, Y. M. Zhang, K. Dzepina, J. R. Kimmel, D. Sueper, J. T. Jayne, S. C. Herndon, A. M. Trimborn, L. R. Williams, E. C. Wood, A. M. Middlebrook, C. E. Kolb, U. Baltensperger, D. R. Worsnop, Evolution of organic aerosols in the atmosphere. *Science* **326**, 1525–1529 (2009).
4. M. O. Andreae, D. Rosenfeld, Aerosol-cloud-precipitation interactions. Part 1. The nature and sources of cloud-active aerosols. *Earth. Sci. Rev.* **89**, 13–41 (2008).
5. T. M. VanReken, N. L. Ng, R. C. Flagan, J. H. Seinfeld, Cloud condensation nucleus activation properties of biogenic secondary organic aerosol. *J. Geophys. Res. Atmos.* **110**, D07206 (2005).
6. D. F. Zhao, A. Buchholz, R. Tillmann, E. Kleist, C. Wu, F. Rubach, A. Kiendler-Scharr, Y. Rudich, J. Wildt, T. F. Mentel, Environmental conditions regulate the impact of plants on cloud formation. *Nat. Commun.* **8**, 14067 (2017).
7. K. E. H. Hartz, T. Rosenorn, S. R. Ferchak, T. M. Raymond, M. Bilde, N. M. Donahue, S. N. Pandis, Cloud condensation nuclei activation of monoterpene and sesquiterpene secondary organic aerosol. *J. Geophys. Res. Atmos.* **110**, D14208 (2005).
8. K. Tsigaridis, M. Kanakidou, The present and future of secondary organic aerosol direct forcing on climate. *Curr. Clim. Change. Rep.* **4**, 84–98 (2018).
9. C. E. Scott, A. Rap, D. V. Spracklen, P. M. Forster, K. S. Carslaw, G. W. Mann, K. J. Pringle, N. Kivekas, M. Kulmala, H. Lihavainen, P. Tunved, The direct and indirect radiative effects of biogenic secondary organic aerosol. *Atmos. Chem. Phys.* **14**, 447–470 (2014).
10. M. Hallquist, J. C. Wenger, U. Baltensperger, Y. Rudich, D. Simpson, M. Claeys, J. Dommen, N. M. Donahue, C. George, A. H. Goldstein, J. F. Hamilton, H. Herrmann, T. Hoffmann, Y. Iinuma, M. Jang, M. E. Jenkin, J. L. Jimenez, A. Kiendler-Scharr, W. Maenhaut, G. McFiggans, T. F. Mentel, A. Monod, A. S. H. Prevot, J. H. Seinfeld, J. D. Surratt, R. Szmigielski, J. Wildt, The formation, properties and impact of secondary organic aerosol: Current and emerging issues. *Atmos. Chem. Phys.* **9**, 5155–5236 (2009).
11. M. Ehn, J. A. Thornton, E. Kleist, M. Sipilä, H. Junninen, I. Pullinen, M. Springer, F. Rubach, R. Tillmann, B. Lee, F. Lopez-Hilfiker, S. Andres, I. H. Acir, M. Rissanen, T. Jokinen, S. Schobesberger, J. Kangasluoma, J. Kontkanen, T. Nieminen, T. Kurtén, L. B. Nielsen, S. Jørgensen, H. G. Kjaergaard, M. Canagaratna, M. D. Maso, T. Berndt, T. Petäjä, A. Wahner, V. M. Kerminen, M. Kulmala, D. R. Worsnop, J. Wildt, T. F. Mentel, A large source of low-volatility secondary organic aerosol. *Nature* **506**, 476–479 (2014).
12. J. Kirkby, J. Duplissy, K. Sengupta, C. Frege, H. Gordon, C. Williamson, M. Heinritzi, M. Simon, C. Yan, J. Almeida, J. Trostl, T. Nieminen, I. K. Ortega, R. Wagner, A. Adamov, A. Amorim, A. K. Bernhammer, F. Bianchi, M. Breitenlechner, S. Brilke, X. M. Chen, J. Craven, A. Dias, S. Ehrhart, R. C. Flagan, A. Franchin, C. Fuchs, R. Guida, J. Hakala, C. R. Hoyle, T. Jokinen, H. Junninen, J. Kangasluoma, J. Kim, M. Krapf, A. Kurten, A. Laaksonen, K. Lehtipalo, V. Makhmutov, S. Mathot, U. Molteni, A. Onnela, O. Peräkylä, F. Piel, T. Petäjä, A. P. Praplan, K. Pringle, A. Rap, N. A. D. Richards, I. Riipinen, M. P. Rissanen, L. Rondo, N. Sarnela, S. Schobesberger, C. E. Scott, J. H. Seinfeld, M. Sipila, G. Steiner, Y. Stozhkov, F. Stratmann, A. Tome, A. Virtanen, A. L. Vogel, A. C. Wagner, P. E. Wagner, E. Weingartner, D. Wimmer, P. M. Winkler, P. L. Ye, X. Zhang, A. Hansel, J. Dommen, N. M. Donahue, D. R. Worsnop, U. Baltensperger, M. Kulmala, K. S. Carslaw, J. Curtius, Ion-induced nucleation of pure biogenic particles. *Nature* **533**, 521–526 (2016).
13. J. Tröstl, W. K. Chuang, H. Gordon, M. Heinritzi, C. Yan, U. Molteni, L. Ahlm, C. Frege, F. Bianchi, R. Wagner, M. Simon, K. Lehtipalo, C. Williamson, J. S. Craven, J. Duplissy, A. Adamov, J. Almeida, A. K. Bernhammer, M. Breitenlechner, S. Brilke, A. Dias, S. Ehrhart, R. C. Flagan, A. Franchin, C. Fuchs, R. Guida, M. Gysel, A. Hansel, C. R. Hoyle, T. Jokinen, H. Junninen, J. Kangasluoma, H. Keskinen, J. Kim, M. Krapf, A. Kurten, A. Laaksonen, M. Lawler, M. Leiminger, S. Mathot, O. Möhler, T. Nieminen, A. Onnela, T. Petäjä, F. M. Piel, P. Miettinen, M. P. Rissanen, L. Rondo, N. Sarnela, S. Schobesberger, K. Sengupta, M. Sipilä, J. N. Smith, G. Steiner, A. Tomè, A. Virtanen, A. C. Wagner, E. Weingartner, D. Wimmer, P. M. Winkler, P. L. Ye, K. S. Carslaw, J. Curtius, J. Dommen, J. Kirkby, M. Kulmala, I. Riipinen, D. R. Worsnop, N. M. Donahue, U. Baltensperger, The role of low-volatility organic compounds in initial particle growth in the atmosphere. *Nature* **533**, 527–531 (2016).
14. C. Mohr, J. A. Thornton, A. Heitto, F. D. Lopez-Hilfiker, A. Lutz, I. Riipinen, J. Hong, N. M. Donahue, M. Hallquist, T. Petäjä, M. Kulmala, T. Yli-Juuti, Molecular identification of organic vapors driving atmospheric nanoparticle growth. *Nat. Commun.* **10**, 4442 (2019).
15. G. McFiggans, T. F. Mentel, J. Wildt, I. Pullinen, S. Kang, E. Kleist, S. Schmitt, M. Springer, R. Tillmann, C. Wu, D. F. Zhao, M. Hallquist, C. Faxon, M. Le Breton, A. M. Hallquist, D. Simpson, R. Bergstrom, M. E. Jenkin, M. Ehn, J. A. Thornton, M. R. Alfarra, T. J. Bannan, C. J. Percival, M. Priestley, D. Topping, A. Kiendler-Scharr, Secondary organic aerosol reduced by mixture of atmospheric vapours. *Nature* **565**, 587–593 (2019).
16. P. Roldin, M. Ehn, T. Kurtén, T. Olenius, M. P. Rissanen, N. Sarnela, J. Elm, P. Rantala, L. Q. Hao, N. Hyttinen, L. Heikkinen, D. R. Worsnop, L. Pichelstorfer, C. Xavier, P. Clusius, E. Öström, T. Petäjä, M. Kulmala, H. Vehkamäki, A. Virtanen, I. Riipinen, M. Boy, The role of highly oxygenated organic molecules in the boreal aerosol-cloud-climate system. *Nat. Commun.* **10**, 4370 (2019).
17. C. Rose, Q. Zha, L. Dada, C. Yan, K. Lehtipalo, H. Junninen, S. B. Mazon, T. Jokinen, N. Sarnela, M. Sipilä, T. Petäjä, V.-M. Kerminen, F. Bianchi, M. Kulmala, Observations of biogenic ion-induced cluster formation in the atmosphere. *Sci. Adv.* **4**, eaar5218 (2018).
18. F. Bianchi, T. Kurtén, M. Riva, C. Mohr, M. P. Rissanen, P. Roldin, T. Berndt, J. D. Crounse, P. O. Wennberg, T. F. Mentel, J. Wildt, H. Junninen, T. Jokinen, M. Kulmala, D. R. Worsnop, J. A. Thornton, N. Donahue, H. G. Kjaergaard, M. Ehn, Highly oxygenated organic molecules (HOM) from gas-phase autoxidation involving peroxy radicals: A key contributor to atmospheric aerosol. *Chem. Rev.* **119**, 3472–3509 (2019).
19. J. D. Crounse, L. B. Nielsen, S. Jørgensen, H. G. Kjaergaard, P. O. Wennberg, Autoxidation of organic compounds in the atmosphere. *J. Phys. Chem. Lett.* **4**, 3513–3520 (2013).
20. S. Iyer, M. P. Rissanen, R. Valiev, S. Barua, J. E. Krechmer, J. Thornton, M. Ehn, T. Kurtén, Molecular mechanism for rapid autoxidation in α-pinene ozonolysis. *Nat. Commun.* **12**, 878 (2021).
21. T. Jokinen, T. Berndt, R. Makkonen, V. M. Kerminen, H. Junninen, P. Paasonen, F. Stratmann, H. Herrmann, A. B. Guenther, D. R. Worsnop, M. Kulmala, M. Ehn, M. Sipilä, Production of extremely low volatile organic compounds from biogenic emissions: Measured yields and atmospheric implications. *Proc. Natl. Acad. Sci. U.S.A.* **112**, 7123–7128 (2015).
22. S. Tomaz, D. Wang, N. Zabalegui, D. Li, H. Lamkaddam, F. Bachmeier, A. Vogel, M. E. Monge, S. Perrier, U. Baltensperger, C. George, M. Rissanen, M. Ehn, I. El Haddad, M. Riva, Structures and reactivity of peroxy radicals and dimeric products revealed by online tandem mass spectrometry. *Nat. Commun.* **12**, 300 (2021).
23. U. Molteni, M. Simon, M. Heinritzi, C. R. Hoyle, A. K. Bernhammer, F. Bianchi, M. Breitenlechner, S. Brilke, A. Dias, J. Duplissy, C. Frege, H. Gordon, C. Heyn, T. Jokinen, A. Kurten, K. Lehtipalo, V. Makhmutov, T. Petäjä, S. M. Pieber, A. P. Praplan, S. Schobesberger, G. Steiner, Y. Stozhkov, A. Tomé, J. Tröstl, A. C. Wagner, R. Wagner, C. Williamson, C. Yan, U. Baltensperger, J. Curtius, N. M. Donahue, A. Hansel, J. Kirkby, M. Kulmala, D. R. Worsnop, J. Dommen, Formation of highly oxygenated organic molecules from α-pinene ozonolysis: Chemical characteristics, mechanism, and kinetic model development. *ACS Earth Space Chem.* **3**, 873–883 (2019).
24. A. B. Guenther, X. Jiang, C. L. Heald, T. Sakulyanontvittaya, T. Duhl, L. K. Emmons, X. Wang, The model of emissions of gases and aerosols from nature version 2.1 (MEGAN2.1): An extended and updated framework for modeling biogenic emissions. *Geosci. Model Dev.* **5**, 1471–1492 (2012).
25. T. Berndt, Peroxy radical processes and product formation in the OH radical-initiated oxidation of α-pinene for near-atmospheric conditions. *J. Phys. Chem. A* **125**, 9151–9160 (2021).
26. T. Berndt, S. Richters, T. Jokinen, N. Hyttinen, T. Kurtén, R. V. Otkjær, H. G. Kjaergaard, F. Stratmann, H. Herrmann, M. Sipilä, M. Kulmala, M. Ehn, Hydroxyl radical-induced formation of highly oxidized organic compounds. *Nat. Commun.* **7**, 13677 (2016).
27. L. Xu, K. H. Møller, J. D. Crounse, R. V. Otkjær, H. G. Kjaergaard, P. O. Wennberg, Unimolecular reactions of peroxy radicals formed in the oxidation of α-pinene and β-pinene by hydroxyl radicals. *J. Phys. Chem. A* **123**, 1661–1674 (2019).
28. J. Peeters, L. Vereecken, G. Fantechi, The detailed mechanism of the OH-initiated atmospheric oxidation of α-pinene: A theoretical study. *Phys. Chem. Chem. Phys.* **3**, 5489–5504 (2001).
29. L. Vereecken, J. Peeters, Theoretical study of the formation of acetone in the OH-initiated atmospheric oxidation of α-pinene. *J. Phys. Chem. A* **104**, 11140–11146 (2000).
30. L. Vereecken, J. F. Müller, J. Peeters, Low-volatility poly-oxygenates in the OH-initiated atmospheric oxidation of alpha-pinene: Impact of non-traditional peroxyl radical chemistry. *Phys. Chem. Chem. Phys.* **9**, 5241–5248 (2007).
31. E. Praske, R. V. Otkjaer, J. D. Crounse, J. C. Hethcox, B. M. Stoltz, H. G. Kjaergaard, P. O. Wennberg, Atmospheric autoxidation is increasingly important in urban and suburban North America. *Proc. Natl. Acad. Sci. U.S.A.* **115**, 64–69 (2018).
32. J. J. Orlando, G. S. Tyndall, Laboratory studies of organic peroxy radical chemistry: An overview with emphasis on recent issues of atmospheric significance. *Chem. Soc. Rev.* **41**, 6294–6317 (2012).

33. J. Peeters, S. Vandenberk, E. Piessens, V. Pultau, H-atom abstraction in reactions of cyclic polyalkenes with OH. *Chemosphere* **38**, 1189–1195 (1999).
34. L. Vereecken, J. Peeters, Enhanced H-atom abstraction from pinonaldehyde, pinonic acid, pinic acid, and related compounds: Theoretical study of C–H bond strengths. *Phys. Chem. Chem. Phys.* **4**, 467–472 (2002).
35. C. Rio, P. M. Flaud, J. C. Loison, E. Villenave, Experimental revaluation of the importance of the abstraction channel in the reactions of monoterpenes with OH radicals. *Chem. Phys. Chem.* **11**, 3962–3970 (2010).
36. L. Vereecken, J. Peeters, H-atom abstraction by OH-radicals from (biogenic) (poly) alkenes: C-H bond strengths and abstraction rates. *Chem. Phys. Lett.* **333**, 162–168 (2001).
37. T. F. Mentel, M. Springer, M. Ehn, E. Kleist, I. Pullinen, T. Kurten, M. Rissanen, A. Wahner, J. Wildt, Formation of highly oxidized multifunctional compounds: Autoxidation of peroxy radicals formed in the ozonolysis of alkenes—Deduced from structure-product relationships. *Atmos. Chem. Phys.* **15**, 6745–6765 (2015).
38. D. F. Zhao, S. H. Schmitt, M. J. Wang, I. H. Acir, R. Tillmann, Z. F. Tan, A. Novelli, H. Fuchs, I. Pullinen, R. Wegener, F. Rohrer, J. Wildt, A. Kiendler-Scharr, A. Wahner, T. F. Mentel, Effects of NO_x and SO_2 on the secondary organic aerosol formation from photooxidation of α-pinene and limonene. *Atmos. Chem. Phys.* **18**, 1611–1628 (2018).
39. N. Hyttinen, O. Kupiainen-Määttä, M. P. Rissanen, M. Muuronen, M. Ehn, T. Kurtén, Modeling the charging of highly oxidized cyclohexene ozonolysis products using nitrate-based chemical ionization. *J. Phys. Chem. A* **119**, 6339–6345 (2015).
40. N. Hyttinen, M. P. Rissanen, T. Kurtén, Computational comparison of acetate and nitrate chemical ionization of highly oxidized cyclohexene ozonolysis intermediates and products. *J. Phys. Chem. A* **121**, 2172–2179 (2017).
41. I. Pullinen, S. Schmitt, S. Kang, M. Sarrafzadeh, P. Schlag, S. Andres, E. Kleist, T. F. Mentel, F. Rohrer, M. Springer, R. Tillmann, J. Wildt, C. Wu, D. F. Zhao, A. Wahner, A. Kiendler-Scharr, Impact of NO_x on secondary organic aerosol (SOA) formation from α-pinene and β-pinene photooxidation: The role of highly oxygenated organic nitrates. *Atmos. Chem. Phys.* **20**, 10125–10147 (2020).
42. T. Berndt, W. Scholz, B. Mentler, L. Fischer, H. Herrmann, M. Kulmala, A. Hansel, Accretion product formation from self- and cross-reactions of RO_2 radicals in the atmosphere. *Angew. Chem. Int. Edit.* **57**, 3820–3824 (2018).
43. Y. Zhao, J. A. Thornton, H. O. T. Pye, Quantitative constraints on autoxidation and dimer formation from direct probing of monoterpene-derived peroxy radical chemistry. *Proc. Natl. Acad. Sci. U.S.A.* **115**, 12142–12147 (2018).
44. H. Shen, D. Zhao, I. Pullinen, S. Kang, L. Vereecken, H. Fuchs, I.-H. Acir, R. Tillmann, F. Rohrer, J. Wildt, A. Kiendler-Scharr, A. Wahner, T. F. Mentel, Highly oxygenated organic nitrates formed from NO_3 radical-initiated oxidation of β-pinene. *Environ. Sci. Technol.* **55**, 15658–15671 (2021).
45. J. Wildt, T. F. Mentel, A. Kiendler-Scharr, T. Hoffmann, S. Andres, M. Ehn, E. Kleist, P. Musgen, F. Rohrer, Y. Rudich, M. Springer, R. Tillmann, A. Wahner, Suppression of new particle formation from monoterpene oxidation by NO_x. *Atmos. Chem. Phys.* **14**, 2789–2804 (2014).
46. C. Yan, W. Nie, A. L. Vogel, L. Dada, K. Lehtipalo, D. Stolzenburg, R. Wagner, M. P. Rissanen, M. Xiao, L. Ahonen, L. Fischer, C. Rose, F. Bianchi, H. Gordon, M. Simon, M. Heinritzi, O. Garmash, P. Roldin, A. Dias, P. Ye, V. Hofbauer, A. Amorim, P. S. Bauer, A. Bergen, A. K. Bernhammer, M. Breitenlechner, S. Brilke, A. Buchholz, S. B. Mazon, M. R. Canagaratna, X. Chen, A. Ding, J. Dommen, D. C. Draper, J. Duplissy, C. Frege, C. Heyn, R. Guida, J. Hakala, L. Heikkinen, C. R. Hoyle, T. Jokinen, J. Kangasluoma, J. Kirkby, J. Kontkanen, A. Kurten, M. J. Lawler, H. Mai, S. Mathot, R. L. Mauldin, U. Molteni, L. Nichman, T. Nieminen, J. Nowak, A. Ojdanic, A. Onnela, A. Pajunoja, T. Petaja, F. Piel, L. L. J. Quelever, N. Sarnela, S. Schallhart, K. Sengupta, M. Sipila, A. Tome, J. Trostl, O. Vaisanen, A. C. Wagner, A. Ylisirnio, Q. Zha, U. Baltensperger, K. S. Carslaw, J. Curtius, R. C. Flagan, A. Hansel, I. Riipinen, J. N. Smith, A. Virtanen, P. M. Winkler, N. M. Donahue, V. M. Kerminen, M. Kulmala, M. Ehn, D. R. Worsnop, Size-dependent influence of NO_x on the growth rates of organic aerosol particles. *Sci. Adv.* **6**, eaay4945 (2020).
47. K. Lehtipalo, C. Yan, L. Dada, F. Bianchi, M. Xiao, R. Wagner, D. Stolzenburg, L. R. Ahonen, A. Amorim, A. Baccarini, P. S. Bauer, B. Baumgartner, A. Bergen, A.-K. Bernhammer, M. Breitenlechner, S. Brilke, A. Buchholz, S. B. Mazon, D. Chen, X. Chen, A. Dias, J. Dommen, D. C. Draper, J. Duplissy, M. Ehn, H. Finkenzeller, L. Fischer, C. Frege, C. Fuchs, O. Garmash, H. Gordon, J. Hakala, X. He, L. Heikkinen, M. Heinritzi, J. C. Helm, V. Hofbauer, C. R. Hoyle, T. Jokinen, J. Kangasluoma, V.-M. Kerminen, C. Kim, J. Kirkby, J. Kontkanen, A. Kürten, M. J. Lawler, H. Mai, S. Mathot, R. L. Mauldin, U. Molteni, L. Nichman, W. Nie, T. Nieminen, A. Ojdanic, A. Onnela, M. Passananti, T. Petäjä, F. Piel, V. Pospisilova, L. L. J. Quéléver, M. P. Rissanen, C. Rose, N. Sarnela, S. Schallhart, S. Schuchmann, K. Sengupta, M. Simon, M. Sipilä, C. Tauber, A. Tomé, J. Tröstl, O. Väisänen, A. L. Vogel, R. Volkamer, A. C. Wagner, M. Wang, L. Weitz, D. Wimmer, P. Ye, A. Ylisirniö, Q. Zha, K. S. Carslaw, J. Curtius, N. M. Donahue, R. C. Flagan, A. Hansel, I. Riipinen, A. Virtanen, P. M. Winkler, U. Baltensperger, M. Kulmala, D. R. Worsnop, Multicomponent new particle formation from sulfuric acid, ammonia, and biogenic vapors. *Sci. Adv.* **4**, eaau5363 (2018).
48. S. M. Saunders, M. E. Jenkin, R. G. Derwent, M. J. Pilling, Protocol for the development of the Master Chemical Mechanism, MCM v3 (Part A): Tropospheric degradation of non-aromatic volatile organic compounds. *Atmos. Chem. Phys.* **3**, 161–180 (2003).
49. K. H. Møller, R. V. Otkjær, J. Chen, H. G. Kjaergaard, Double bonds are key to fast unimolecular reactivity in first-generation monoterpene hydroxy peroxy radicals. *J. Phys. Chem. A* **124**, 2885–2896 (2020).
50. L. Vereecken, B. Nozière, H migration in peroxy radicals under atmospheric conditions. *Atmos. Chem. Phys.* **20**, 7429–7458 (2020).
51. L. Vereecken, J. Peeters, Decomposition of substituted alkoxy radicals—Part I: A generalized structure-activity relationship for reaction barrier heights. *Phys. Chem. Chem. Phys.* **11**, 9062–9074 (2009).
52. F. Rohrer, B. Bohn, T. Brauers, D. Bruning, F. J. Johnen, A. Wahner, J. Kleffmann, Characterisation of the photolytic HONO-source in the atmosphere simulation chamber SAPHIR. *Atmos. Chem. Phys.* **5**, 2189–2201 (2005).
53. K. H. Møller, K. H. Bates, H. G. Kjaergaard, The importance of peroxy radical hydrogen-shift reactions in atmospheric isoprene oxidation. *J. Phys. Chem. A* **123**, 920–932 (2019).
54. S. Jørgensen, H. C. Knap, R. V. Otkjær, A. M. Jensen, M. L. H. Kjeldsen, P. O. Wennberg, H. G. Kjaergaard, Rapid hydrogen shift scrambling in hydroperoxy-substituted organic peroxy radicals. *J. Phys. Chem. A* **120**, 266–275 (2016).
55. E. Praske, R. V. Otkjær, J. D. Crounse, J. C. Hethcox, B. M. Stoltz, H. G. Kjaergaard, P. O. Wennberg, Intramolecular hydrogen shift chemistry of hydroperoxy-substituted peroxy radicals. *J. Phys. Chem. A* **123**, 590–600 (2019).
56. L. Vereecken, G. Vu, A. Wahner, A. Kiendler-Scharr, H. M. T. Nguyen, A structure activity relationship for ring closure reactions in unsaturated alkylperoxy radicals. *Phys. Chem. Chem. Phys.* **23**, 16564–16576 (2021).
57. S. Kang, "Formation of highly oxygenated organic molecules from α-pinene photochemistry", thesis, University of Wuppertal (2021).
58. T. Berndt, N. Hyttinen, H. Herrmann, A. Hansel, First oxidation products from the reaction of hydroxyl radicals with isoprene for pristine environmental conditions. *Commun. Chem.* **2**, 21 (2019).
59. M. Riva, P. Rantala, J. E. Krechmer, O. Peräkylä, Y. Zhang, L. Heikkinen, O. Garmash, C. Yan, M. Kulmala, D. Worsnop, M. Ehn, Evaluating the performance of five different chemical ionization techniques for detecting gaseous oxygenated organic species. *Atmos. Meas. Tech.* **12**, 2403–2421 (2019).
60. T. Jokinen, M. Sipila, H. Junninen, M. Ehn, G. Lonn, J. Hakala, T. Petaja, R. L. Mauldin, M. Kulmala, D. R. Worsnop, Atmospheric sulphuric acid and neutral cluster measurements using CI-APi-TOF. *Atmos. Chem. Phys.* **12**, 4117–4125 (2012).
61. F. L. Eisele, D. J. Tanner, Measurement of the gas phase concentration of H_2SO_4 and methane sulfonic acid and estimates of H_2SO_4 production and loss in the atmosphere. *J. Geophys. Res. Atmos.* **98**, 9001–9010 (1993).
62. S. M. Aschmann, R. Atkinson, Rate constants for the gas-phase reactions of alkanes with Cl atoms at 296 ± 2 K. *Int. J. Chem. Kinet.* **27**, 613–622 (1995).
63. C. G. Masoud, L. H. Ruiz, Chlorine-initiated oxidation of α-pinene: Formation of secondary organic aerosol and highly oxygenated organic molecules. *ACS Earth Space Chem.* **5**, 2307–2319 (2021).
64. Y. H. Wang, M. Riva, H. B. Xie, L. Heikkinen, S. Schallhart, Q. Z. Zha, C. Yan, X. C. He, O. Perakyla, M. Ehn, Formation of highly oxygenated organic molecules from chlorine-atom-initiated oxidation of alpha-pinene. *Atmos. Chem. Phys.* **20**, 5145–5155 (2020).
65. T. Berndt, K. H. Møller, H. Herrmann, H. G. Kjaergaard, Trimethylamine outruns terpenes and aromatics in atmospheric autoxidation. *J. Phys. Chem. A* **125**, 4454–4466 (2021).
66. C. Yan, W. Nie, M. Aijala, M. P. Rissanen, M. R. Canagaratna, P. Massoli, H. Junninen, T. Jokinen, N. Sarnela, S. A. K. Hame, S. Schobesberger, F. Canonaco, L. Yao, A. S. H. Prévôt, T. Petäjä, M. Kulmala, M. Sipilä, D. R. Worsnop, M. Ehn, Source characterization of highly oxidized multifunctional compounds in a boreal forest environment using positive matrix factorization. *Atmos. Chem. Phys.* **16**, 12715–12731 (2016).
67. T. Jokinen, J. Kontkanen, K. Lehtipalo, H. E. Manninen, J. Aalto, A. Porcar-Castell, O. Garmash, T. Nieminen, M. Ehn, J. Kangasluoma, H. Junninen, J. Levula, J. Duplissy, L. R. Ahonen, P. Rantala, L. Heikkinen, C. Yan, M. Sipilä, D. R. Worsnop, J. Bäck, T. Petäjä, V.-M. Kerminen, M. Kulmala, Solar eclipse demonstrating the importance of photochemistry in new particle formation. *Sci. Rep.* **7**, 45707 (2017).
68. P. Massoli, H. Stark, M. R. Canagaratna, J. E. Krechmer, L. Xu, N. L. Ng, R. L. Mauldin, C. Yan, J. Kimmel, P. K. Misztal, J. L. Jimenez, J. T. Jayne, D. R. Worsnop, Ambient measurements of highly oxidized gas-phase molecules during the Southern Oxidant and Aerosol Study (SOAS) 2013. *ACS Earth Space Chem.* **2**, 653–672 (2018).
69. H. O. T. Pye, E. L. D'Ambro, B. Lee, S. Schobesberger, M. Takeuchi, Y. Zhao, F. Lopez-Hilfiker, J. M. Liu, J. E. Shilling, J. Xing, R. Mathur, A. M. Middlebrook, J. Liao, A. Welti, M. Graus, C. Warneke, J. A. de Gouw, J. S. Holloway, T. B. Ryerson, I. B. Pollack, J. A. Thornton, Anthropogenic enhancements to production of highly oxygenated molecules from autoxidation. *Proc. Natl. Acad. Sci. U.S.A.* **116**, 6641–6646 (2019).
70. R. Atkinson, J. Arey, Atmospheric degradation of volatile organic compounds. *Chem. Rev.* **103**, 4605–4638 (2003).

71. A. Hofzumahaus, F. Rohrer, K. D. Lu, B. Bohn, T. Brauers, C. C. Chang, H. Fuchs, F. Holland, K. Kita, Y. Kondo, X. Li, S. R. Lou, M. Shao, L. M. Zeng, A. Wahner, Y. H. Zhang, Amplified trace gas removal in the troposphere. *Science* **324**, 1702–1704 (2009).
72. I. R. Piletic, T. E. Kleindienst, Rates and yields of unimolecular reactions producing highly oxidized peroxy radicals in the OH-induced autoxidation of α-pinene, β-pinene, and limonene. *J. Phys. Chem. A* **126**, 88–100 (2022).
73. Z. D. Wang, M. Ehn, M. P. Rissanen, O. Garmash, L. Quéléver, L. L. Xing, M. Monge-Palacios, P. Rantala, N. M. Donahue, T. Berndt, S. M. Sarathy, Efficient alkane oxidation under combustion engine and atmospheric conditions. *Commun. Chem.* **4**, 18 (2021).
74. E. L. D'Ambro, N. Hyttinen, K. H. Møller, S. Iyer, R. V. Otkjær, D. M. Bell, J. Liu, F. D. Lopez-Hilfiker, S. Schobesberger, J. E. Shilling, A. Zelenyuk, H. G. Kjaergaard, J. A. Thornton, T. Kurtén, Pathways to highly oxidized products in the Δ3-carene + OH system. *Environ. Sci. Technol.* **56**, 2213–2224 (2022).
75. B. Bohn, F. Rohrer, T. Brauers, A. Wahner, Actinometric measurements of NO_2 photolysis frequencies in the atmosphere simulation chamber SAPHIR. *Atmos. Chem. Phys.* **5**, 493–503 (2005).
76. D. F. Zhao, I. Pullinen, H. Fuchs, S. Schrade, R. R. Wu, I. H. Acir, R. Tillmann, F. Rohrer, J. Wildt, Y. D. Guo, A. Kiendler-Scharr, A. Wahner, S. Kang, L. Vereecken, T. F. Mentel, Highly oxygenated organic molecule (HOM) formation in the isoprene oxidation by NO_3 radical. *Atmos. Chem. Phys.* **21**, 9681–9704 (2021).
77. D. F. Zhao, M. Kaminski, P. Schlag, H. Fuchs, I. H. Acir, B. Bohn, R. Haseler, A. Kiendler-Scharr, F. Rohrer, R. Tillmann, M. J. Wang, R. Wegener, J. Wildt, A. Wahner, T. F. Mentel, Secondary organic aerosol formation from hydroxyl radical oxidation and ozonolysis of monoterpenes. *Atmos. Chem. Phys.* **15**, 991–1012 (2015).
78. M. P. Rissanen, T. Kurtén, M. Sipilä, J. A. Thornton, J. Kangasluoma, N. Sarnela, H. Junninen, S. Jørgensen, S. Schallhart, M. K. Kajos, R. Taipale, M. Springer, T. F. Mentel, T. Ruuskanen, T. Petäjä, D. R. Worsnop, H. G. Kjaergaard, M. Ehn, The formation of highly oxidized multifunctional products in the ozonolysis of cyclohexene. *J. Am. Chem. Soc.* **136**, 15596–15606 (2014).
79. H. Fuchs, H. P. Dorn, M. Bachner, B. Bohn, T. Brauers, S. Gomm, A. Hofzumahaus, F. Holland, S. Nehr, F. Rohrer, R. Tillmann, A. Wahner, Comparison of OH concentration measurements by DOAS and LIF during SAPHIR chamber experiments at high OH reactivity and low NO concentration. *Atmos. Meas. Tech.* **5**, 1611–1626 (2012).
80. R. Atkinson, D. L. Baulch, R. A. Cox, J. N. Crowley, R. F. Hampson, R. G. Hynes, M. E. Jenkin, M. J. Rossi, J. Troe, Evaluated kinetic and photochemical data for atmospheric chemistry: Volume I—Gas phase reactions of O_x, NO_x and SO_x species. *Atmos. Chem. Phys.* **4**, 1461–1738 (2004).
81. Y. L. Huang, R. Zhao, S. M. Charan, C. M. Kenseth, X. Zhang, J. H. Seinfeld, Unified theory of vapor-wall mass transport in Teflon-walled environmental chambers. *Environ. Sci. Technol.* **52**, 2134–2142 (2018).
82. P. J. Ziemann, R. Atkinson, Kinetics, products, and mechanisms of secondary organic aerosol formation. *Chem. Soc. Rev.* **41**, 6582–6605 (2012).
83. M. E. Jenkin, S. M. Saunders, M. J. Pilling, The tropospheric degradation of volatile organic compounds: A protocol for mechanism development. *Atmos. Environ.* **31**, 81–104 (1997).
84. N. C. Eddingsaas, C. L. Loza, L. D. Yee, J. H. Seinfeld, P. O. Wennberg, α-pinene photooxidation under controlled chemical conditions—Part 1: Gas-phase composition in low- and high-NO_x environments. *Atmos. Chem. Phys.* **12**, 6489–6504 (2012).
85. M. Rolletter, M. Kaminski, I. H. Acir, B. Bohn, H. P. Dorn, X. Li, A. Lutz, S. Nehr, F. Rohrer, R. Tillmann, R. Wegener, A. Hofzumahaus, A. Kiendler-Scharr, A. Wahner, H. Fuchs, Investigation of the α-pinene photooxidation by OH in the atmospheric simulation chamber SAPHIR. *Atmos. Chem. Phys.* **19**, 11635–11649 (2019).
86. B. R. Larsen, D. Di Bella, M. Glasius, R. Winterhalter, N. R. Jensen, J. Hjorth, Gas-phase OH oxidation of monoterpenes: Gaseous and particulate products. *J. Atmos. Chem.* **38**, 231–276 (2001).
87. B. Nozière, I. Barnes, K. H. Becker, Product study and mechanisms of the reactions of α-pinene and of pinonaldehyde with OH radicals. *J. Geophys. Res. Atmos.* **104**, 23645–23656 (1999).
88. Y. Zhao, D. G. Truhlar, The M06 suite of density functionals for main group thermochemistry, thermochemical kinetics, noncovalent interactions, excited states, and transition elements: Two new functionals and systematic testing of four M06-class functionals and 12 other functionals. *Theor. Chem. Acc.* **120**, 215–241 (2008).
89. T. H. Dunning, Gaussian basis sets for use in correlated molecular salculations. I. The atoms boron through neon and hydrogen. *J. Chem. Phys.* **90**, 1007–1023 (1989).
90. S. Grimme, S. Ehrlich, L. Goerigk, Effect of the damping function in dispersion corrected density functional theory. *J. Comput. Chem.* **32**, 1456–1465 (2011).
91. L. Goerigk, A. Hansen, C. Bauer, S. Ehrlich, A. Najibi, S. Grimme, A look at the density functional theory zoo with the advanced GMTKN55 database for general main group thermochemistry, kinetics and noncovalent interactions. *Phys. Chem. Chem. Phys.* **19**, 32184–32215 (2017).
92. I. M. Alecu, J. J. Zheng, Y. Zhao, D. G. Truhlar, Computational thermochemistry: Scale factor databases and scale factors for vibrational frequencies obtained from electronic model chemistries. *J. Chem. Theory Comput.* **6**, 2872–2887 (2010).
93. T. H. Dunning, K. A. Peterson, A. K. Wilson, Gaussian basis sets for use in correlated molecular calculations. X. The atoms aluminum through argon revisited. *J. Chem. Phys.* **114**, 9244–9253 (2001).
94. R. J. Bartlett, G. D. Purvis, Many-body perturbation theory, coupled-pair many-electron theory, and the importance of quadruple excitations for the correlation problem. *Int. J. Quantum Chem.* **14**, 561–581 (1978).
95. M. J. Frisch, G. W. Trucks, H. B. Schlegel, G. E. Scuseria, M. A. Robb, J. R. Cheeseman, G. Scalmani, V. Barone, G. A. Petersson, H. Nakatsuji, X. Li, M. Caricato, A. V. Marenich, J. Bloino, B. G. Janesko, R. Gomperts, B. Mennucci, H. P. Hratchian, J. V. Ortiz, A. F. Izmaylov, J. L. Sonnenberg, D. Williams-Young, F. Ding, F. Lipparini, F. Egidi, J. Goings, B. Peng, A. Petrone, T. Henderson, D. Ranasinghe, V. G. Zakrzewski, J. Gao, N. Rega, G. Zheng, W. Liang, M. Hada, M. Ehara, K. Toyota, R. Fukuda, J. Hasegawa, M. Ishida, T. Nakajima, Y. Honda, O. Kitao, H. Nakai, T. Vreven, K. Throssell, J. A. Montgomery Jr., J. E. Peralta, F. Ogliaro, M. J. Bearpark, J. J. Heyd, E. N. Brothers, K. N. Kudin, V. N. Staroverov, T. A. Keith, R. Kobayashi, J. Normand, K. Raghavachari, A. P. Rendell, J. C. Burant, S. S. Iyengar, J. Tomasi, M. Cossi, J. M. Millam, M. Klene, C. Adamo, R. Cammi, J. W. Ochterski, R. L. Martin, K. Morokuma, O. Farkas, J. B. Foresman, D. J. Fox. (Gaussian Inc., Wallingford, CT, 2016).
96. L. Vereecken, J. Peeters, The 1,5-H-shift in 1-butoxy: A case study in the rigorous implementation of transition state theory for a multirotamer system. *J. Chem. Phys.* **119**, 5159–5170 (2003).
97. C. Eckart, The penetration of a potential barrier by electrons. *Phys. Rev.* **35**, 1303–1309 (1930).
98. H. S. Johnston, J. Heicklen, Tunnelling corrections for unsymmetrical Eckart potential energy barriers. *J. Phys. Chem.* **66**, 532–533 (1962).
99. B. Nozière, L. Vereecken, Direct observation of aliphatic peroxy radical autoxidation and water effects: An experimental and theoretical study. *Angew. Chem. Int. Edit.* **58**, 13976–13982 (2019).
100. M. E. Jenkin, R. Valorso, B. Aumont, A. R. Rickard, Estimation of rate coefficients and branching ratios for reactions of organic peroxy radicals for use in automated mechanism construction. *Atmos. Chem. Phys.* **19**, 7691–7717 (2019).
101. L. Vereecken, J. Peeters, A structure-activity relationship for the rate coefficient of H-migration in substituted alkoxy radicals. *Phys. Chem. Chem. Phys.* **12**, 12608–12620 (2010).
102. A. Novelli, C. Cho, H. Fuchs, A. Hofzumahaus, F. Rohrer, R. Tillmann, A. Kiendler-Scharr, A. Wahner, L. Vereecken, Experimental and theoretical study on the impact of a nitrate group on the chemistry of alkoxy radicals. *Phys. Chem. Chem. Phys.* **23**, 5474–5495 (2021).
103. H. C. Knap, S. Jørgensen, Rapid hydrogen shift reactions in acyl peroxy radicals. *J. Phys. Chem. A* **121**, 1470–1479 (2017).
104. S. Y. Wang, S. M. McNamara, C. W. Moore, D. Obrist, A. Steffen, P. B. Shepson, R. M. Staebler, A. R. W. Raso, K. A. Pratt, Direct detection of atmospheric atomic bromine leading to mercury and ozone depletion. *Proc. Natl. Acad. Sci. U.S.A.* **116**, 14479–14484 (2019).

Acknowledgments: We thank the SAPHIR team including I.-H. Acir, R. Tillmann, F. Rohrer, B. Bonn, and Z. Tan for supporting our experiments and A. Wahner and A. Kiendler-Scharr for providing experiment opportunities and comments. D.Z. would like to thank Y. Zhang for supportive discussion during the manuscript preparation. **Funding:** H.S. and D.Z. would like to thank the funding support of the National Natural Science Foundation of China (41875145, 92044301) and the Science and Technology Commission of Shanghai Municipality (20230711400 and 21230780200). S.K. and T.F.M. acknowledge the support by the EU Project FORCeS (grant agreement no. 821205). **Author contributions:** D.Z. conceptualized the idea with the aid of S.K. and T.F.M. D.Z. and T.F.M. planned the study. D.Z., I.P., and H.F. conducted the data collection. H.S. and S.K. analyzed experimental data. H.S. interpreted the data and conducted box model simulation. L.V. performed the quantum chemical calculation. H.S., D.Z., L.V., and T.F.M. wrote and edited the manuscript and the Supplementary Materials with the input from all authors. All coauthors discussed the results and commented on the manuscript and the Supplementary Materials. **Competing interests:** The authors declare that they have no competing interests. **Data and materials availability:** The quantum chemical data underlying the theoretical kinetic calculations can be found as a text file at https://doi.org/10.26165/JUELICH-DATA/GLU9BW. The experimental data are available at Zenodo (10.5281/zenodo.6787403). All data needed to evaluate the conclusions in the paper are present in the paper and/or the Supplementary Materials.

Submitted 8 March 2022
Accepted 1 September 2022
Published 21 October 2022
10.1126/sciadv.abp8702

ScienceAdvances

Unexpected significance of a minor reaction pathway in daytime formation of biogenic highly oxygenated organic compounds

Hongru ShenLuc VereeckenSungah KangIida PullinenHendrik FuchsDefeng ZhaoThomas F. Mentel

Sci. Adv., 8 (42), eabp8702. • DOI: 10.1126/sciadv.abp8702

Science Advances (ISSN) is published by the American Association for the Advancement of Science. 1200 New York Avenue NW, Washington, DC 20005. The title *Science Advances* is a registered trademark of AAAS.